Corrosion Science 179 (2021) 109131

Contents lists available at ScienceDirect

Corrosion Science

journal homepage: www.elsevier.com/locate/corsci

Inhibitive effect of sodium carbonate on corrosion of AZ31 magnesium alloy in NaCl solution

L. Prince [a,*], M-A. Rousseau [a], X. Noirfalise [b], L. Dangreau [b], L.B. Coelho [a], M.-G. Olivier [a,b]

[a] Materials Science Department, UMONS-University of Mons, Place du parc 20, B-7000 Mons, Belgium
[b] Materia Nova asbl, Avenue Copernic 3, B-7000 Mons, Belgium

ARTICLE INFO

Keywords:
A. Magnesium
B. Polarization
B. EIS
B. XPS
C. Passive film

ABSTRACT

Magnesium is the world's lightest structural metal, with a significant growth potential in view of the accelerating demand for light-weighting portable devices and transportation (aerospace, automotive), amongst other. The effect of carbonate ions on corrosion protection of AZ31 magnesium alloy was studied in 0.1 M NaCl solution saturated in $Mg(OH)_2$ using Electrochemical Impedance Spectroscopy (EIS), potentiodynamic polarization measurements, hydrogen evolution tests and SEM-EDX analysis. X-ray Photoelectron Spectroscopy (XPS) was used in order to investigate the top-surface composition. The inhibitive effect of CO_3^{2-} ions on corrosion of AZ31 magnesium alloy was highlighted and the underlying mechanisms discussed.

1. Introduction

Considerations concerning energy consumption and environmental issues have convinced the scientific and economic communities to focus on the use of low-density metals which would allow the weight reduction of cars or other vehicles. The ultimate result would be the limitation of fuel consumption and thus greenhouse gas emissions [1,2]. Nowadays, magnesium alloys have a high growth potential in view of the increasing demand for light-weighting portable devices and transportation (aerospace, automotive). Magnesium (Mg) is one of the most abundant elements in the earth's crust. It has a high strength- to- weight ratio with a density of 1740 kg/m^3 and a Young's modulus of 44 GPa. In addition, these alloys present other interesting properties such as a high thermal conductivity, electromagnetic damping protection, machinability and recyclability [3]. The microstructure of AZ31, of nominal composition: 3 % Al, 1 % Zn and 0.3 % Mn (wt %) with the balance Mg, has been comprehensively characterized [4] and the influence of the intermetallic phases on corrosion behavior explained in terms of their nobility. Although Mg-Al alloys are well known to form a $Mg_{17}Al_{12}$ β phase, the aluminum content of AZ31 is insufficient to allow the formation of this particular intermetallic [5]. Consequently, most of Al remains in solid solution in the majority alpha phase, along with the alloyed Zn. The principal type of intermetallic present in AZ31 alloy is Al-Mn phase, dispersed both in the α-Mg grains and at grain boundaries as particles of typical size between 2 and 20 μm [6].

However, the high chemical reactivity and therefore the low corrosion resistance of magnesium alloys in aggressive environments limit their applications [7]. The E-pH diagram of pure magnesium established by Pourbaix in 1963 indicates that the standard electrochemical potential of magnesium is -2.37 V vs SHE [8]. This means that magnesium is directly oxidized in aqueous electrolyte. Different stable chemical species of magnesium are expected depending on pH of the solution. In acidic or neutral media, magnesium is oxidized to the free Mg^{2+} ion [9]. In basic medium, the formation of $Mg(OH)_2$ film is thermodynamically stable [9], but the passive layer formed is not sufficiently protective, presenting a Pilling-Bedworth ratio (ratio of the volume of metal oxide to the metal) of 0.81 for MgO/Mg. This value lower than 1 is an indication that the surface oxide layer is porous [10].

The coating technology related to the corrosion protection of magnesium is a topical challenge. Surface conditioning treatments and different types of coatings are under current investigation to fulfil the requirements related to the envisaged for applications and corrosion exposure scenarios. The take-off of Mg-based technologies relies on the appropriate application of efficient corrosion inhibitors to coating surface treatments. However, only a limited number of chemical compounds have been reported until recently to be effective for Mg alloys [11]. The 2p orbital of Mg being fully occupied, limits the acceptance of electrons from donor molecules forming stable chemical bonds [12]. Cr (VI) was traditionally used for corrosion protection strategies of Mg alloys [13]. Nonetheless, hexavalent chromium is extremely irritating,

* Corresponding author.
E-mail address: loic.prince@umons.ac.be (L. Prince).

https://doi.org/10.1016/j.corsci.2020.109131
Received 14 April 2020; Received in revised form 23 September 2020; Accepted 10 November 2020
Available online 12 November 2020

toxic, caustic and harmful to the environment [14]. Fluorides [4], nitrates [15], phosphates [16] and silicates [17] have been proven as suitable inorganic inhibitors for Mg alloys. The inhibiting effect of most of inorganic substances could be correlated with the formation of chemical conversion films that seal the intrinsic defects of the magnesium hydroxide/oxide layers [18,19]. Concerning rare earth salts, $CeCl_3$ and $LaCl_3$ tend to accelerate the corrosion of magnesium alloys [11,20], which is completely opposite to the results obtained from $Ce(NO_3)_3$ and $La(NO_3)_3$ on AZ63 and AM60 alloys [19,21]. Hence, the corrosion inhibition effects of $Ce(NO_3)_3$ and $La(NO_3)_3$ were attributed to the presence of nitrate rather than the rare earth element. When the dissolution of Mg and local alkalization of the electrolyte occurred very rapidly due to high surface area of Mg, Ce^{3+} or La^{3+} did not allow a sufficient increase of pH on the Mg surface in order to stabilize $Mg(OH)_2$. Moreover, the OH^- ions formed by water reduction reaction are consumed to form $Ce(OH)_3/Ce(OH)_4$ and $La(OH)_3$ in the diffusion layer/bulk solution, rather than on the Mg surface [11].

The presence of CO_2 in the atmosphere affects the corrosion mechanism of magnesium alloys in a humid environment. The concentration of CO_2 in the natural ambient air can be estimated to be 330 ppm [22]. CO_2 dissolution in water forms carbonic acid reducing the electrolyte pH at the metal surface [22]:

$$CO_2 + H_2O \rightleftharpoons HCO_3^- + H^+,\ pK_a = 6.65 \quad (1)$$

$$HCO_3^- + H_2O \rightleftharpoons CO_3^{2-} + H_3O^+,\ pKa = 10.33 \quad (2)$$

$$Mg(OH)_2(s) \rightleftharpoons Mg^{2+}(aq) + 2(OH^-)(aq),\ K_S = 10^{-11} \quad (3)$$

$$2\ Mg^{2+}(aq) + CO_3^{2-}(aq) + 2OH\text{-} + 3H_2O \rightarrow Mg_2(OH)_2CO_3.\ 3H_2O\ (s),\ \log K_s = -18.4 \quad (4)$$

[22]

In a humid atmosphere, CO_3^{2-} ions can be generated through the reaction between carbon dioxide and moisture (Eqs. (1) and (2)) [23,24], resulting in the formation of a magnesium hydroxycarbonate film ($Mg_2(OH)_2CO_3.\ 3H_2O$) (Eqs. (3) and (4)). As a result of the carbonate layer, the corrosion rate is reported to decrease [22]. However, the thickness and the compacity of the carbonated film should be higher than magnesium hydroxide to enhance the corrosion resistance of magnesium alloy [25,26].

In NaCl solution, CO_2 also plays a significant role on corrosion of AZ31 alloy. Qu et al. [27] found that the corrosion rate of AZ31 was higher in NaCl solution saturated with CO_2 than without CO_2, probably due to the increased conductivity and lower pH. In un-buffered chloride solution, in the absence of CO_2, the local pH on the Mg surface rapidly increases to 10.3 due to the low solubility of $Mg(OH)_2$ [28]. Nevertheless, the inhibitive effect of CO_2 was also revealed versus immersion time, by the formation of an insoluble corrosion product comprising $Mg_2(OH)_2CO_3$ (s) accumulated on the AZ31 surface, creating a protective layer whose thickness increased with time.

Gulbrandsen noted that the corrosion rate of magnesium was dependent on the HCO_3^- concentration, affecting the quality of the corrosion products covering the surface [29]. Xin et al. [30] suggested that HCO_3^- ions could induce a rapid surface passivation when magnesium carbonate precipitates and completely suppresses pitting corrosion. Zeng et al. [31] demonstrated that the hydrogen evolution rate decreased with decreasing bicarbonate concentration. The corrosion rate slowed down in saline solution with a 4.17 mmol/l HCO_3^- concentration but increased when the concentration in HCO_3^- ions reached 11.91 mmol/l. The presence of bicarbonate ions significantly decreased the open-circuit potential of AZ31.

Nonetheless, from our knowledge, there is no study related to the investigation of the inhibitive action of CO_3^{2-} ions on AZ31 magnesium alloys. The present work aims at investigating the effect of carbonate ions on the corrosion protection of AZ31 magnesium alloy in 0.1 M NaCl solutions saturated with $Mg(OH)_2$. Electrochemical Impedance Spectroscopy, potentiodynamic polarization measurements and SEM-EDX analysis are employed. X-ray Photoelectron Spectroscopy is used in order to determine the surface composition of the outermost surface. The inhibitive effect of CO_3^{2-} could thus be highlighted.

2. Experimental

2.1. Materials and sample preparation

AZ31 magnesium alloy sheets were supplied by KG Fridman AB (SWEDEN), with the following composition: 2.5–3.5 % Al, 0.7–1.3 % Zn, 0.2 % Mn, 0.05 % Si, 0.05 % Cu, 0.04 % Ca, 0.005 % Fe, 0.1 % Ni (wt %) and Mg rest. All samples were degreased in 1 M NaOH for 120 s, rinsed with distilled water, etched in 2 M HNO_3 solution for 30 s, immersed in 0.25 M HNO_3 solution for 60 s and, finally, rinsed with distilled water before drying in air.

Sodium carbonate (Na_2CO_3 (98 %)) was obtained from Alpha Aesar. The solutions were aqueous 0.1 M NaCl saturated with $Mg(OH)_2$ and containing different Na_2CO_3 concentrations: 5 mM, 25 mM and 50 mM, respectively. The sodium carbonate solubility is 212.5 g/l (Alpha Aesar). The saturated solution had a stable pH value equal to 10.3 and was chosen in order to avoid pH changes with time evolution.

2.2. Electrochemical measurements

2.2.1. Electrochemical impedance spectroscopy

The corrosion resistance of the bare samples in the different electrolytes was studied by using electrochemical impedance spectroscopy versus immersion time. The stability of open circuit potential (OCP) was checked for 6 h before EIS measurements. EIS spectra were determined in a frequency range from 100 kHz to 100 mHz using a Parstat Model 2273 controlled by Powersuite® software. The EIS data at low frequencies (10^{-3}–10^{-2} Hz) are highly scattered due to fast dissolution of magnesium substrate leading to non-stationarities. A conventional three-electrode electrochemical cell was used, composed of an Ag/AgCl/KCl saturated reference electrode, a platinum counter-electrode and a working electrode, namely the studied sample. The sample area in contact with the electrolyte was 7 cm^2. The electrochemical cell was placed in a faraday cage in order to minimize external electromagnetic interferences on the system. The inhibition efficiency, was calculated using the following equation (Eq. (5)) [32]:

$$IE(\%) = \frac{|Z|^{inh}_{10^{-1}Hz} - |Z|^{0}_{10^{-1}Hz}}{|Z|^{inh}_{10^{-1}Hz}} \times 100\ \% \quad (5)$$

where $|Z|^{inh}_{10^{-1}Hz}$ is the modulus at low frequency with inhibitor and, $|Z|^{0}_{10^{-1}Hz}$ is the modulus at low frequency without the testing molecule for a same immersion time in the electrolyte.

The Commercial software ZSimpWin was utilized for analyzing the obtained impedance spectra.

2.2.2. Potentiodynamic polarizations

Potentiodynamic polarizations were performed in 0.1 M NaCl solution saturated in $Mg(OH)_2$ with or without Na_2CO_3 salt using a Parstat Model 2273 controlled by Powersuite® software. The samples, with a surface area of 7 cm^2, were polarized using a sweep rate of 50 mV/min and a sweep range of ±200 mV starting from OCP. The anodic and cathodic polarizations were performed on separate samples. The measurements were performed at least twice for each anodic and cathodic curve in order to ensure reproducibility.

2.3. Morphology characterization

Corrosion products were observed using SEM-FEG (Hitachi SU8020 with cold cathode) and coupled to an energy dispersive X-ray

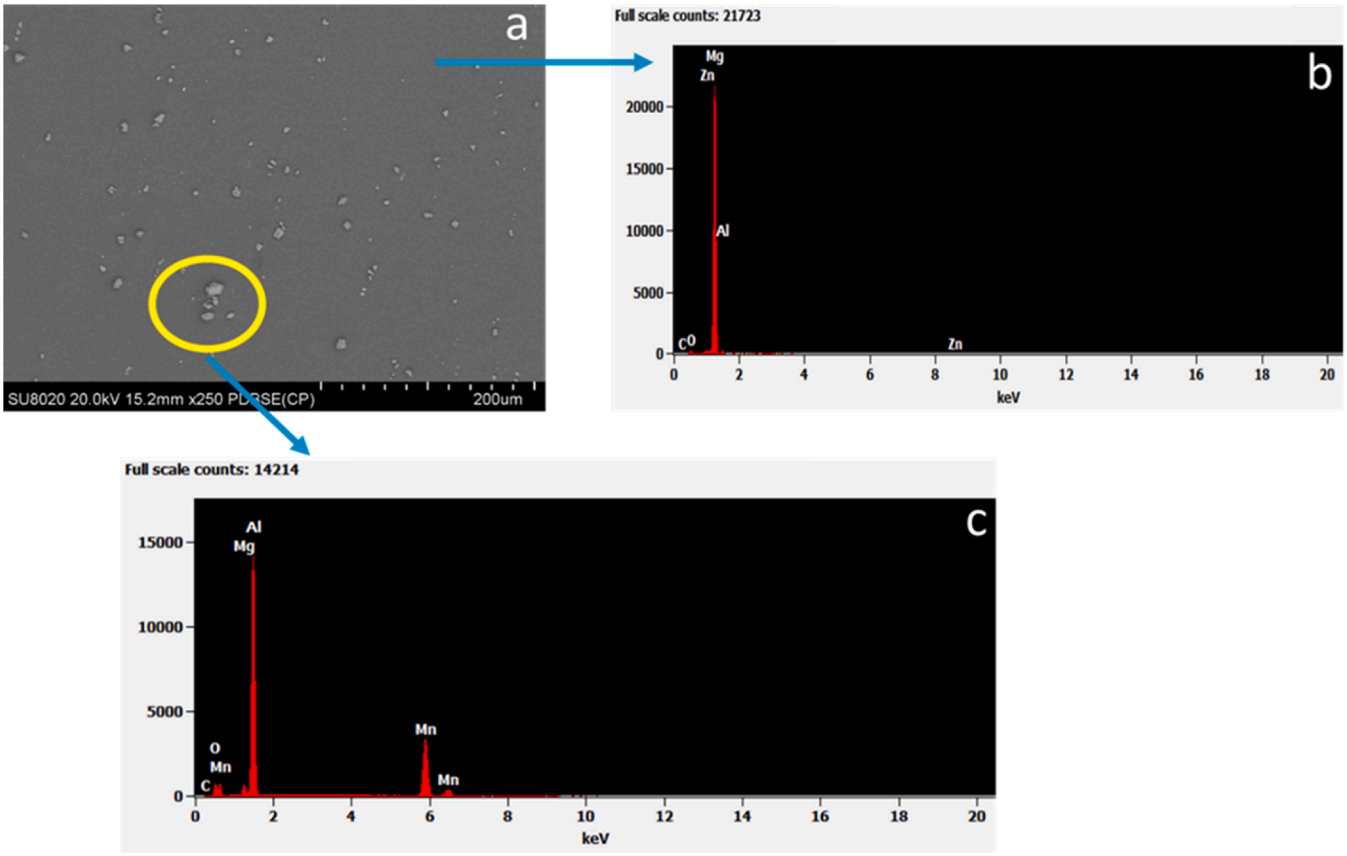

Fig. 1. SEM-FEG (a) micrography of the microstructure of AZ31 (b) EDX spectra from a region without intermetallic compounds (c) EDX spectra from an intermetallic compounds-containing region.

spectrometer analyzer (EDX) to investigate the elemental distribution in the observed micrographs.

2.4. Hydrogen evolution

Hydrogen evolution tests were carried out upon 7 cm^2 area of AZ31 using eudiometers. Unlike typical burette-funnel setup, eudiometers are an enclosed system that prevents the interference (CO_2 and O_2) from ambient environment. All tests were performed for 24 h without interruption and the volume of released hydrogen was recorded visually. All experiments were conducted at room temperature. The volume of H_2 resided in eudiometer and dissolved in the aqueous medium were not considered, since the solubility of H_2 in water is about 0.0016 g/l at room temperature at 1 atm. The inhibition efficiency (IE_H) based on H_2 evolution was calculated using the following equation (Eq. (6)):

$$IE(\ \%) = \frac{V^0_{H_2} - V^{inh}_{H_2}}{V^0_{H_2}} \times 100\ \% \quad (6)$$

In which $V^0_{H_2}$ and $V^{inh}_{H_2}$ are the released H_2 volumes measured during immersion in NaCl solution saturated with $Mg(OH)_2$ without and with the addition of sodium carbonate, respectively.

2.5. Surface analysis

After 7 days of immersion in the electrolytes, AZ31 samples were rinsed with demineralized water and dried with a dehydrated compressed air system. The metallic surface covered by corrosion products was characterized by X-ray photoelectron spectroscopy (XPS). These analyses were carried out with a PHI VERSAPROBE 5000 spectrometer. The measurements were carried out employing an X-Ray source with a spot size of 200 μm and the power of the source was fixed at 50 W. All spectra were shown after energy calibration. The reference peak was C1 s at 285 eV. Quantification was based on the areas of the photoelectron peaks after subtraction of the continuous background approximated by a Shirley baseline.

3. Results

3.1. Morphological characterization

Fig. 1 shows SEM-FEG micrography and corresponding EDX spectra of the AZ31 top surface.

This micrograph (Fig. 1a) clearly shows the presence of particles such as intermetallic compounds. Alloys of Mg-Al are well known to form the $Mg_{17}Al_{12}$ intermetallic phase [33]. Nevertheless, in the case of AZ31 alloy, the Al content is not enough to form this type of intermetallic. Here, the intermetallics were mainly of the Al-Mn type (Fig. 1c), which appeared dispersed in the magnesium matrix (Fig. 1a) [6].

Fig. 2 compares the SEM micrographs of the surface of the tested materials after 7 days of immersion in 0.1 M NaCl solution saturated in $Mg(OH)_2$ without or with sodium carbonate salt. The surface of AZ31 specimens (Fig. 2(a, b, c, d)) was completely covered with a rather uniform and continuous corrosion film. Localized corrosion was also observed (Fig. 2(b)) and this was manifested by the appearance of corrosion pits and large domes of corrosion products. The formation of Al-Mn intermetallic particles can render the α-Mg matrix susceptible to micro galvanic corrosion. It is generally accepted that such particles can act as cathodes for several Mg alloys [6,10]. Microgalvanic coupling of Al_2Mn particles in the AZ31 alloys was shown to cause localized corrosion in the vicinity of the particles in 3.5 % NaCl [6]. The surface of AZ31 with 5 mM Na_2CO_3 (Fig. 2(e, f, g, h)) showed corrosion products with a distinct morphology, characterized by a globular microstructure.

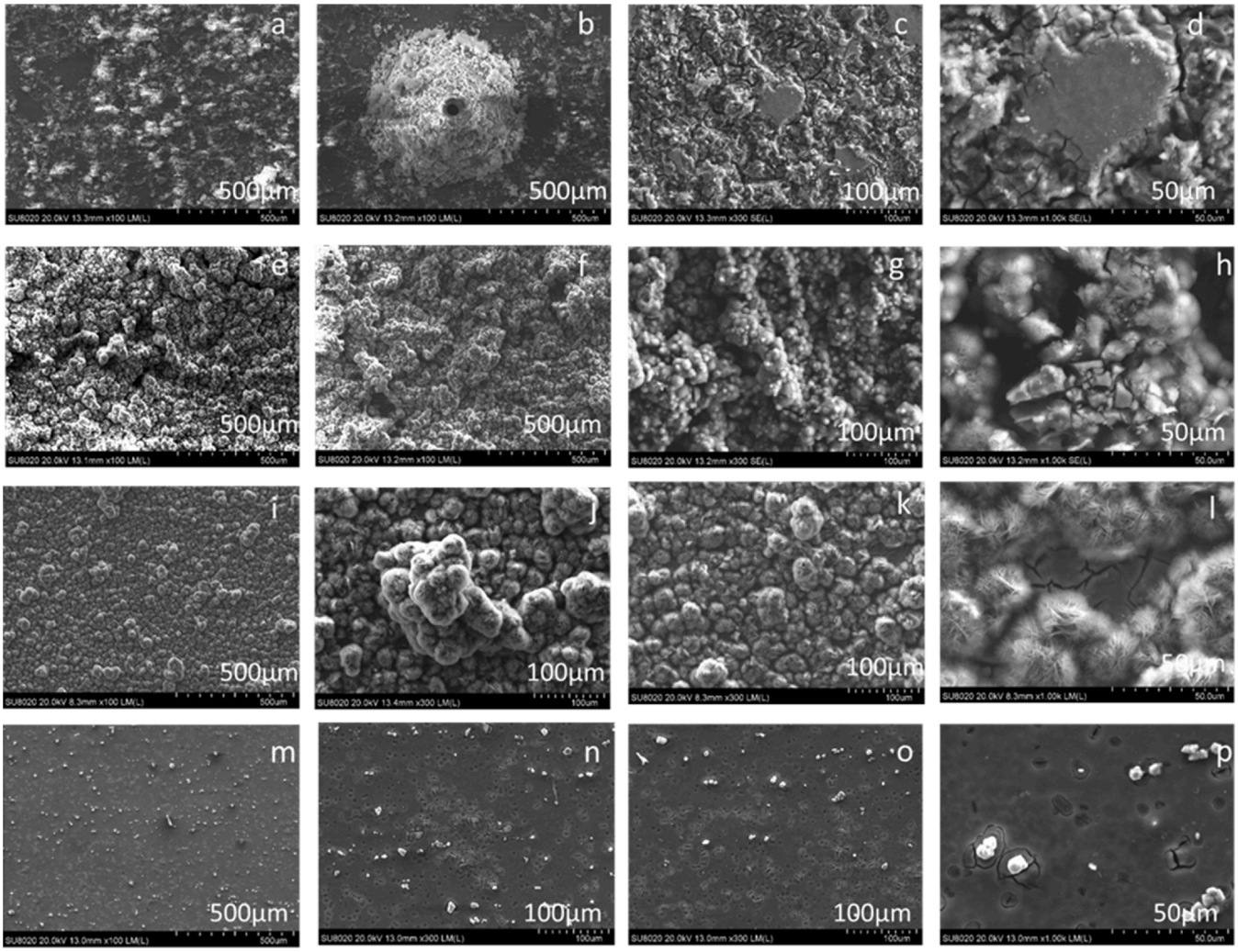

Fig. 2. SEM-FEG micrography of the microstructure of AZ31 after 7 days immersion in 0.1 M NaCl saturated with $Mg(OH)_2$ (reference solution) (a, b, c, d) and in 0.1 M NaCl saturated in $Mg(OH)_2$ with: 5 mM Na_2CO_3 (e, f, g, h), 25 mM Na_2CO_3 (i, j, k, l) and 50 mM Na_2CO_3 (m, n, o, p).

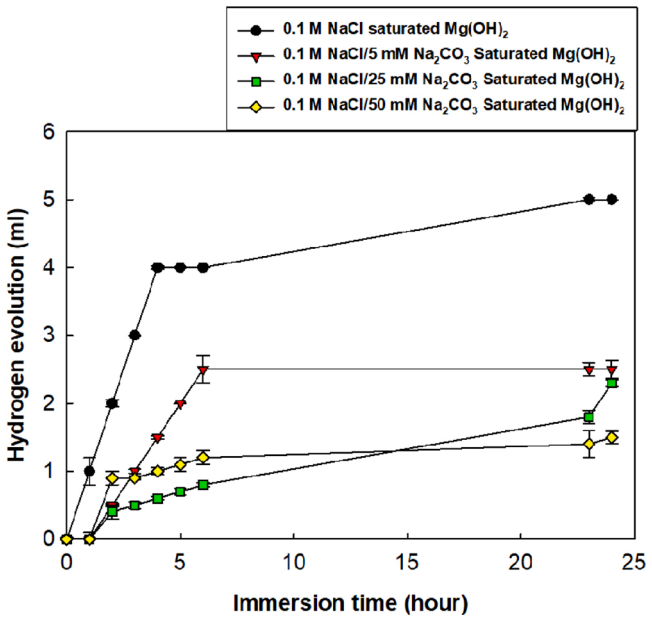

Fig. 3. Hydrogen evolution during 24 h of immersion in 0.1 M NaCl saturated with $Mg(OH)_2$ with or without Na_2CO_3 at different concentrations.

The discontinuous corrosion products associated with the porous morphology of the clusters have certainly allowed a constant exposure of fresh metal. The substrate immersed in NaCl/25 mM Na_2CO_3 (Fig. 2(i, j, k, l)) presented the same morphology of that immersed in NaCl/5 mM Na_2CO_3; but the corrosion products were more uniformly distributed and continuous and needles-like clusters were present. Finally, AZ31 revealed significantly less surface degradation when a concentration of 50 mM Na_2CO_3 was added (Fig. 2(m, n, o, p)). In this latter case, the exposed areas presented micro-cracks that probably resulted from dehydration of hydroxides (such as $Mg(OH)_2$) in the SEM vacuum chamber.

3.2. Hydrogen evolution test

Corrosion of magnesium alloys can be described as an redox process of magnesium oxidation coupled to the reduction and formation of H_2 from both hydrogen ions and/or hydrogen atom in water molecule [34]. The overall reaction of the process can be written as presented in Eq. (7). Theoretically, without considering the minor dissolution in the electrolyte, the hydrogen volume can be directly employed for calculating the consumption rate of Mg alloys [34]. For studying the inhibitive effect of Na_2CO_3 at different concentrations in 0.1 M NaCl saturated with $Mg(OH)_2$, the H_2 volume-time response was recorded (Fig. 3).

$$Mg(s) + 2H_2O(l) \rightarrow Mg(OH)_2(aq) + H_2(g) \quad (7)$$

Table 1
Inhibiting efficiency (IE_H) of Na_2CO_3 tested at different concentrations after 24 h of hydrogen evolution testing.

Concentration (mM)	IE_H (%)
5	45 ± 5.3
25	50 ± 4.2
50	76 ± 2.7

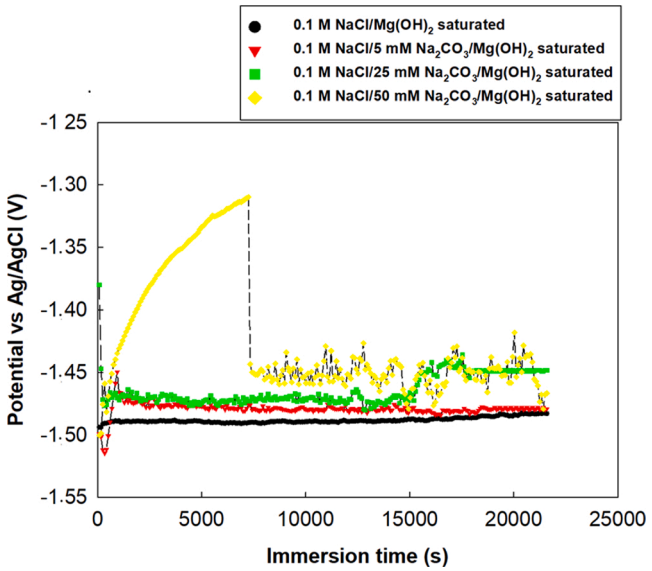

Fig. 4. The open circuit potential (OCP) of AZ31 substrates immersed in 0.1 M NaCl, saturated with $Mg(OH)_2$ with or without Na_2CO_3, at three concentrations (5 mM, 25 mM and 50 mM), measured for 6 h.

From the H_2 volume-time curves presented in (Fig. 3), it could be seen that H_2 production presented a linear behavior within the initial 5 h in the absence of carbonate and for the lowest concentration (5 mM). Next, in these two cases, there was a deceleration of the amount of hydrogen produced, which was related to the simultaneous accumulation of corrosion products on the corroded surface. After that, the volume of evolved H_2 grew in a much lower rate, implying the complete consumption of fresh AZ31 surfaces. The inhibition efficiency (IE_H) of the studied compound, for different concentrations, was determined from the corresponding curves after 24 h of immersion and the obtained values are listed in Table 1:

A positive inhibition efficiency indicates that corrosion is delayed while negative values mean that corrosion is accelerated. By adding Na_2CO_3 at the selected concentrations, the corrosion rate significantly decreased, yielding IE_H between 45 % (5 mM, the lowest concentration) and 76 % (50 mM, the highest concentration). The inhibition efficiency increased accordingly with the inhibitor concentration in the investigated range. The exhaustive study of Lamaka et al. reported a large amount of data on the effectiveness of inhibition in the same saturated electrolyte [11]. By taking that work as a basis for comparison, the achieved inhibition efficiency for Na_2CO_3 which is cheap and eco-responsible has similar efficiency compared to the most promising reported ones.

3.3. Open circuit potential monitoring

The Open Circuit Potentials (OCP) of AZ31 substrates immersed in 0.1 M NaCl saturated with $Mg(OH)_2$ and containing different sodium carbonate concentrations (0, 5, 25 and 50 mM) are presented in Fig. 4.

The OCP for AZ31 in 0.1 M NaCl saturated in $Mg(OH)_2$ stabilized around -1.48 V, already after 30 min. With the addition of Na_2CO_3, however, the OCP curves presented a progressive increase which lasted between 30 min and 120 min, depending on the inhibitor concentration. In 50 mM Na_2CO_3 electrolyte, the highest E shift was observed (~+200 mV), which was reflective of its long period of continuous increase (~120 min). After this transient shift towards more noble potentials, all curves obtained in the presence of carbonate showed an abrupt decrease. At this point, a steady state-like condition was reached and all potentials remained slightly nobler than the potential of AZ31 without inhibitor; around -1.47 V, -1.46 V and -1.44 V for increasing carbonate concentration, respectively. In addition, the higher inhibitor concentration, the spikier was the behavior of the corresponding E curve. The smooth behavior of the E curves during the ennobling period, prior to their sharp decrease, might indicate that the presence of carbonate induced a temporary passivated-like state. The potential decline could thus be related to the rupture of a passive-like film, reflecting the dynamic nature of a competitive process between corrosion and tendency to surface passivation. The EIS and polarization measurements, described in which follows were performed after 6 h of immersion, in order to ensure that the OCP curves have attained a plateau.

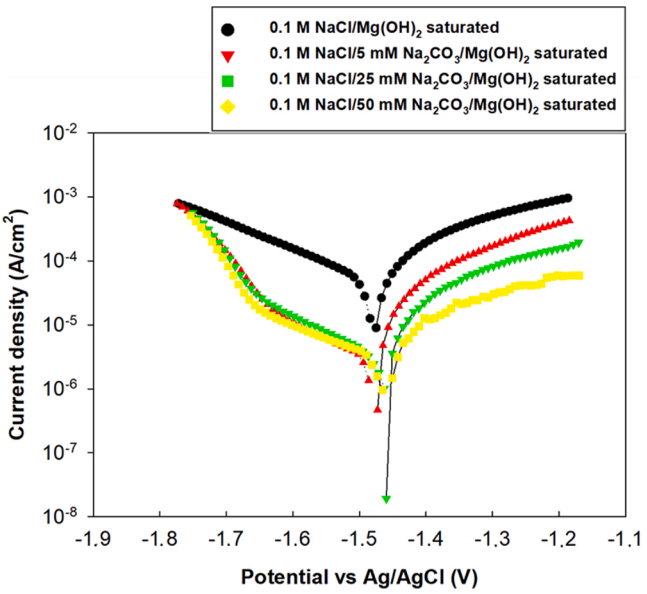

Fig. 5. Potentiodynamic polarization curve of AZ31 substrates immersed in 0.1 M NaCl saturated in $Mg(OH)_2$ with or without Na_2CO_3 inhibitors at different concentrations.

3.4. Potentiodynamic polarization measurements

Potentiodynamic polarization measurements were performed to investigate the corrosion inhibition effect of the testing molecule on the anodic and cathodic reactions (Fig. 5).

Fig. 5 shows the polarization curves of AZ31 obtained after 6 h of exposure to 0.1 M NaCl saturated in $Mg(OH)_2$ for the different tested inhibitor concentrations. A significant decrease in both anodic and cathodic branches was clearly depicted, implying that the corrosion rate slowed down. The current densities (j) measured at OCP were all below 10^{-6}A/cm^2 for the inhibitor-containing media and about 10^{-5}A/cm^2 for the reference solution which represents a significant difference. Concerning the anodic branch, a similar passive-like behavior was observed for all curves. Yet, a clear anodic inhibitive effect dependent on the inhibitor concentration was determined. For instance, at -1.2 V, the j was around 10^{-3}, 5.10^{-4}, 10^{-4} and 5.10^{-5} A/cm^2 for the 0, 5, 25 and 50 mM Na_2CO_3 solutions, respectively. In the case of the cathodic curve in 0.1 M NaCl saturated solution, only the reduction of water (WRR) could be identified as cathodic reaction. With further cathodic potential polarization (potential decrease), the current density gradually increased,

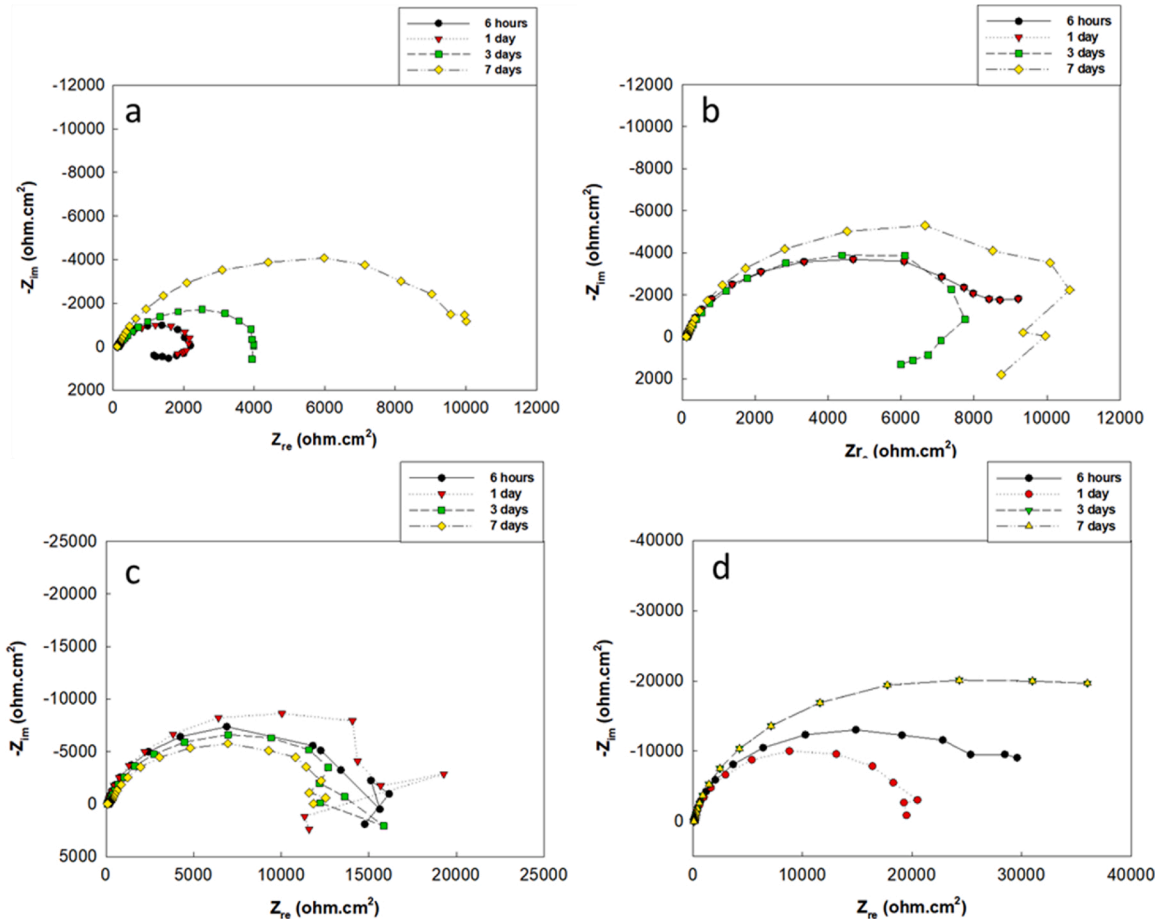

Fig. 6. Nyquist plots of AZ31 substrates immersed in 0.1 M NaCl saturated in $Mg(OH)_2$ without and with inhibitor at different concentrations versus immersion time: (a) 0.1 M NaCl (b) 0.1 M NaCl /5 mM Na_2CO_3 (c) 0.1 M NaCl /25 mM Na_2CO_3, (d) 0.1 M NaCl/50 mM Na_2CO_3.

indicating the enhancement of hydrogen evolution reaction rate. However, the behavior of the cathodic curves greatly changed upon the addition of carbonate salt. In these cases, the cathodic curves comprised two distinct regions: the first one, from the OCP down to ~-1.65 V, was characterized by the same slope of the cathodic curve in the absence of inhibitor; and the second region, from ~-1.65 V down to ~-1.68 V, was marked by a much higher slope. This slope transition certainly represents a change in the mechanism of the cathodic process. If it represents an increase in the kinetics of WRR or the activation of other(s) cathodic reactions (reactional path changes) is a question deserving future investigations. In all cases, the cathodic current density strongly decreased in the presence of sodium carbonate (particularly in the first region of the cathodic curves) and also reduced the extent of hydrogen production. Finally, it is worth noting that the cathodic inhibitive effect was independent on the inhibitor concentration.

3.5. *Electrochemical impedance spectroscopy*

Based on the promising results obtained by the potentiodynamic polarization measurements, electrochemical impedance spectra were determined for AZ31 immersed in each working solution (up to 7 days of immersion). EIS data (Nyquist and Bode diagrams) recorded after consecutive immersion periods (6 h, 1 day, 3 days and 7 days) are given in Figs. 6 and 7 , respectively.

From the Bode diagrams obtained for the AZ31 samples immersed in 0.1 M NaCl (Fig. 7 (a)), it can be seen that the impedance modulus (Z) at low frequency (10^{-1}Hz) remained low with immersion time, varying from 1.10^3 to 9.10^3 ohm. cm^2. These variations were associated with the instability of magnesium oxide/hydroxide layer, subjected to the simultaneous phenomena of growth and dissolution. Moreover, on the Bode phase diagrams, two time constants (TC) could be observed regardless of the immersion time; the first one located in the medium frequency domain and the second one in the low frequency region. The first TC could be associated with the response of the charge transfer resistance and the double layer capacitance at the metal/solution interface, as it presents a phase angle value (from -40° to -60°) characteristic of such capacitive behavior [35]. In addition, the broadening of this time constant over time may be associated with the growth of corrosion products. It is worth noting that the outer layer of corrosion products from aqueous exposure consists mainly of brucite $Mg(OH)_2$, which is predictable because Mg dissolution favors the production of OH- ions from the cathodic reaction. Moreover, the electrolyte is previously saturated $Mg(OH)_2$. Nevertheless, Feliu et al. [35] demonstrated that CO_2 could dissolve in solution and cause the appearance of $MgCO_3$. The low frequency TC (around 20°) corresponded to an inductive loop. According to literature [35–39], this loop is attributed to the high concentration of magnesium ions in relatively film-free areas or with an intermediate step in the corrosion process involving the presence of adsorbed surface species, such as $Mg(OH)^+_{ads}$, $Mg(OH)_{2\ ads}$ and Mg^+_{ads} [40]. Although this approach is formally correct and provides an interpretation of the EIS response, recent experimental works have failed at experimentally revealing the presence of univalent magnesium [41,42].

Concerning the Bode modulus diagrams (Fig. 7(b)) obtained for the samples immersed in 0.1 M NaCl/5 mM Na_2CO_3, the impedance modulus at low frequency remained stable versus immersion time. Z values were higher than in the chloride reference medium, here varying from 6.10^3 to 9.10^3 ohm. cm^2. At low frequency, an inductive behavior

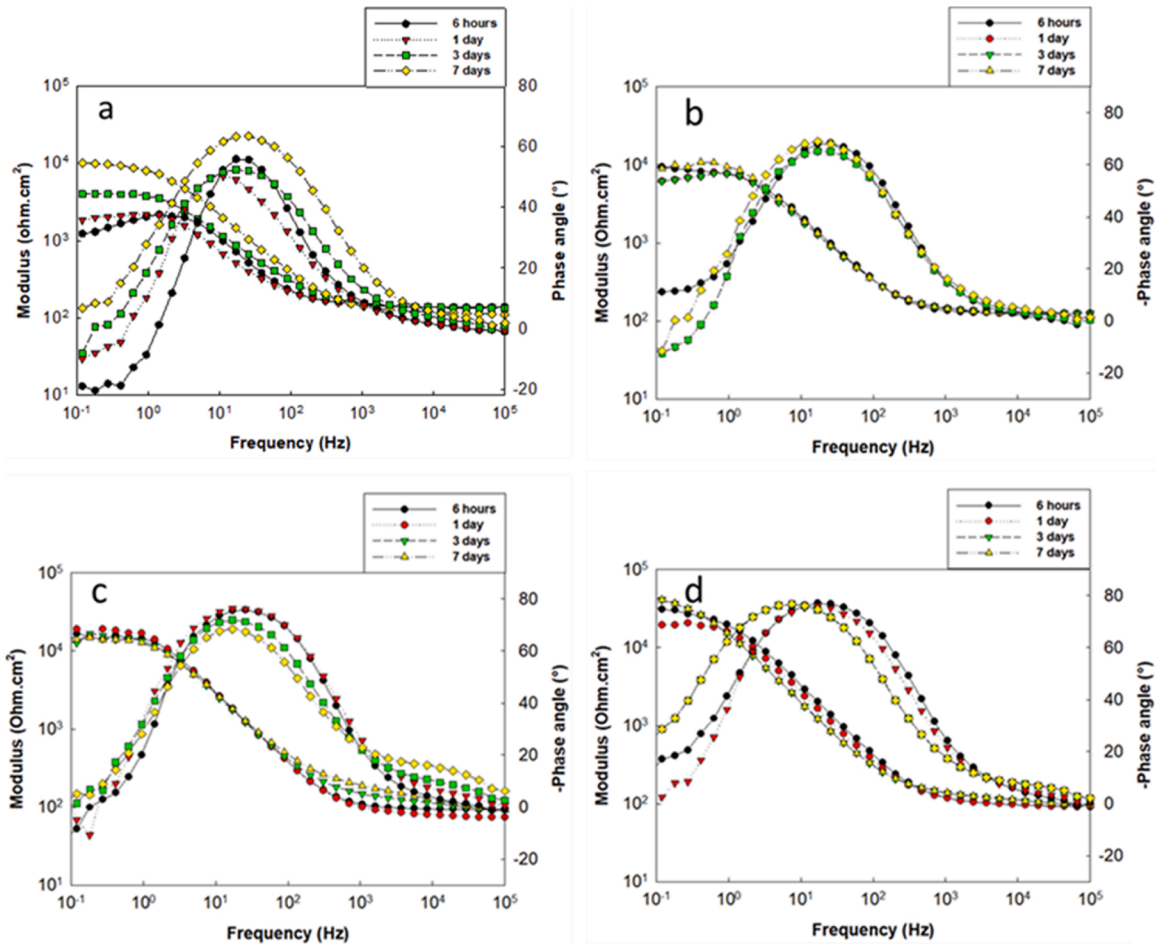

Fig. 7. EIS curves of AZ31 substrates immersed in 0.1 M NaCl saturated in $Mg(OH)_2$ without and with inhibitor at different concentrations versus immersion time: (a) 0.1 M NaCl (b) 0.1 M NaCl /5 mM Na_2CO_3 (c) 0.1 M NaCl /25 mM Na_2CO_3, (d) 0.1 M NaCl/50 mM Na_2CO_3.

was still detected from 3 to 7 days, which points out to the poor protective properties of this layer.

Regarding the Bode diagrams obtained for the samples immersed in 0.1 M NaCl/25 mM and 50 mM Na_2CO_3 (Fig. 7(c and d)), the impedance modulus at low frequency was much higher than in comparison to the reference solution. Indeed, Z values (10^{-1} Hz) varied from 1.10^4 to 2.10^4 ohm. cm^2 and from $3.2.10^4$ to $5.1.10^4$ ohm. cm^2 for increasing carbonate concentrations. Secondly, the capacitive behavior of the medium frequency TC became more marked, attaining phases of -70° and -80° for 25 mM and 50 mM Na_2CO_3, respectively. Moreover, the higher the inhibitor concentration, the less visible was the inductive loop, indicating the decrease of the corresponding corrosion reactions. It can thus be concluded that a protective film, showing a capacitive behavior over a wide range of frequencies, was formed in the highly concentrated carbonate media, remaining stable up to 7 days. It is worth mentioning that, after 3 days of immersion, an additional time constant appeared at the high frequency range, particularly for the 25 mM Na_2CO_3 case. This TC could be associated with the growth of carbonate-based corrosion products which corresponds well with the micrographs presented in Fig. 2(i, j, k, l).

In order to quantify the electrochemical parameters of the inhibiting system, the Bode spectra were fitted with equivalent circuits which have appropriate physical meaning including interface processes of the corroding system. Regarding the overall corrosion processes reflected in EIS spectra, these were fitted by two different equivalent circuits (Fig. 8).

In this circuit (Fig. 8(a)), R_s corresponds to the electrolyte resistance, CPE is the constant phase element relative to the interface phenomenon (electrochemical double layer), R_t is the charge transfer resistance. R is a resistance associated with L the inductance [39]. Secondly, the two-constant spectra were modelled by a series circuit which includes two relaxation processes described by two groups combining of resistor

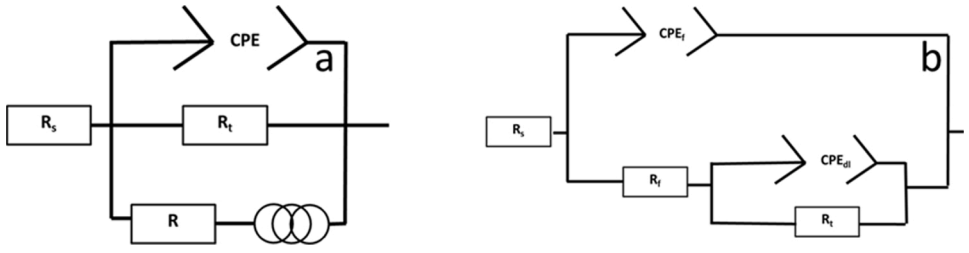

Fig. 8. Equivalent electrical circuits used to fit the EIS experimental data. (a) model a and (b) model b.

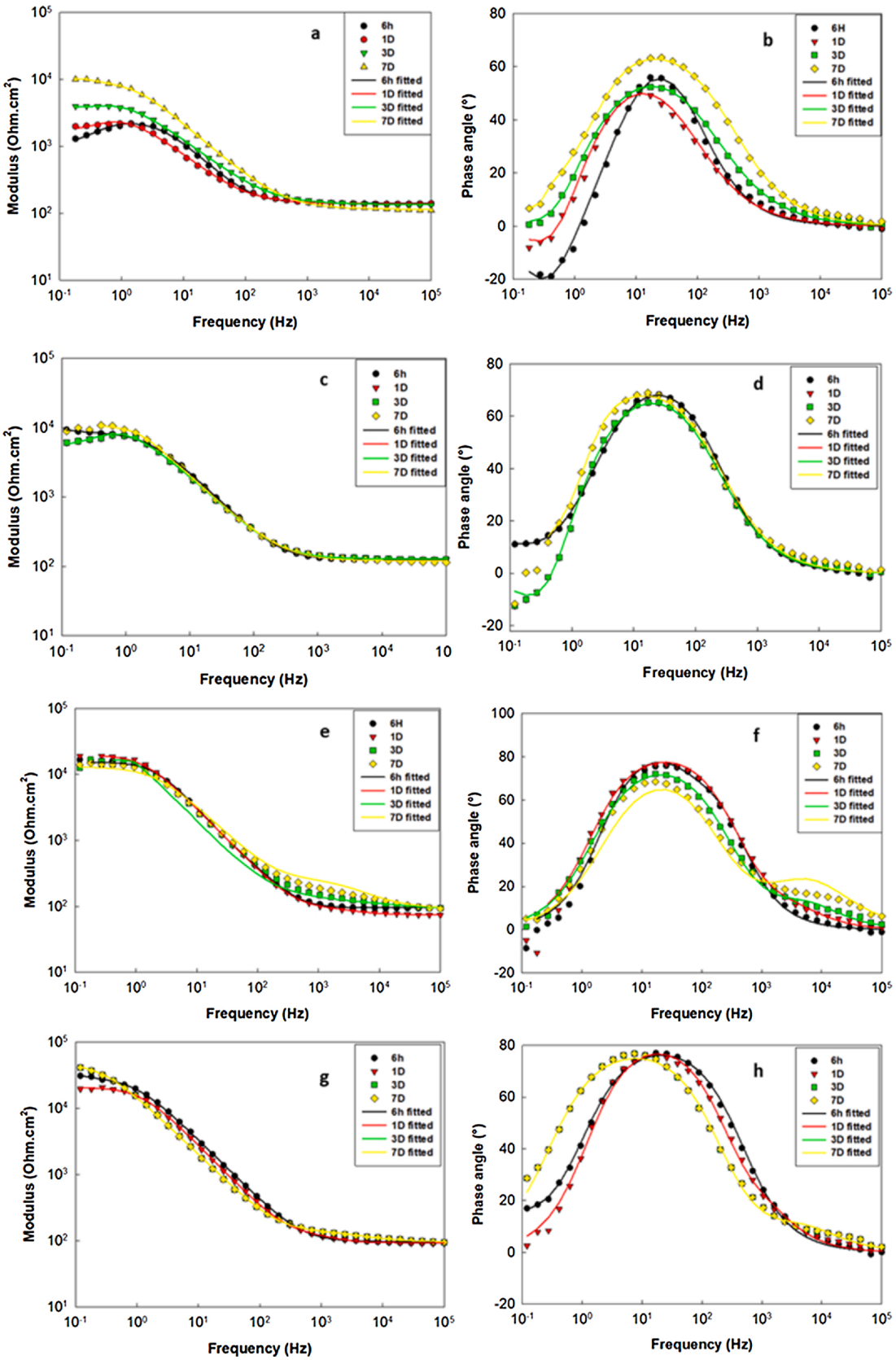

Fig. 9. Impedance modulus (a, c, e, g) and phase angle (b, d, f, h) acquired during immersion in 0.1 M NaCl (a,b) saturated with $Mg(OH)_2$ fitted with model a, 5 mM Na_2CO_3 (c, d) fitted with model a and b, 25 mM Na_2CO_3 (e,f) fitted with model b, 50 mM Na_2CO_3 (g, h) fitted with model b.

Table 2
Results of fitting spectra recorded for AZ31 in the different electrolytes with immersion time.

0.1 M NaCl	Rs(ohm cm^2)	CPE(Fcm^{-2}S^{n-1})	n	Rt(ohm cm^2)	L(Henry)	R(ohm cm^2)
6h	141.8	1.96 10^{-5}	0.91	2217	1103	1542
1d	138.4	4.95 10^{-5}	0.75	2848	1664	3733
3d	134.8	3.31 10^{-5}	0.76	5298	4387	1.30 10^4
7d	114.4	1.64 10^{-5}	0.80	1.49 10^4	1828	3.68 10^4

0.1 M NaCl/5 mM Na_2CO_3	Rs(ohm cm^2)	CPEf(Fcm^{-2}S^{n-1})	n	Rf(ohm cm^2)	CPEdl (Fcm^{-2}S^{n-1})	n	Rt(ohm cm^2)
6h	91.98	7.74 10^{-6}	0.92	6293	2.1 10−3	0.86	4396
1d	124	1.01 10^{-5}	0.90	8707	8.6 10−4	1	2936

	Rs(ohm cm^2)	CPE(Fcm^{-2}S^{n-1})	n	Rt(ohm cm^2)	L(Henry)	R(ohm cm^2)
3d	128.4	1.41 10^{-5}	0.85	9892	7195	1.17 10^4
7d	121.8	1.48 10^{-5}	0.84	2.08 10^4	2431	2.59 10^4

0.1 M NaCl/25 mM Na_2CO_3	Rs(ohm cm^2)	CPEf(Fcm^{-2}S^{n-1})	n	Rf(ohm cm^2)	CPEdl (Fcm^{-2}S^{n-1})	n	Rt(ohm cm^2)
6h	95.47	4.13 10^{-6}	0.99	1700	1.30 10^{-6}	1	1.35 10^4
1d	74.58	2.40 10^{-6}	0.95	45.82	4.12 10−6	0.93	1.96 10^4
3d	94.68	1.87 10^{-6}	0.88	65.02	6.36 10^{-6}	0.90	1.70 10^4
7d	91.39	2.30 10^{-6}	0.78	205.7	5.69 10^{-6}	0.90	1.28 10^4

0.1 M NaCl/50 mM Na_2CO_3	Rs(ohm cm^2)	CPEf(Fcm^{-2}S^{n-1})	n	Rf(ohm cm^2)	CPEdl (Fcm^{-2}S^{n-1})	n	Rt(ohm cm^2)
6h	97.09	6.63 10^{-6}	0.91	2.99 10^4	2.2 10^{-4}	1	1.07 10^4
1d	93.44	3.57 10^{-6}	0.95	118.5	3.55 10^{-6}	0.93	2.06 10^4
3d	97	3.89 10^{-6}	0.84	59.16	8.48 10^{-6}	0.91	4.92 10^4
7d	84.93	2.81 10^{-6}	0.82	86.42	8.98 10^{-6}	0.89	4.95 10^4

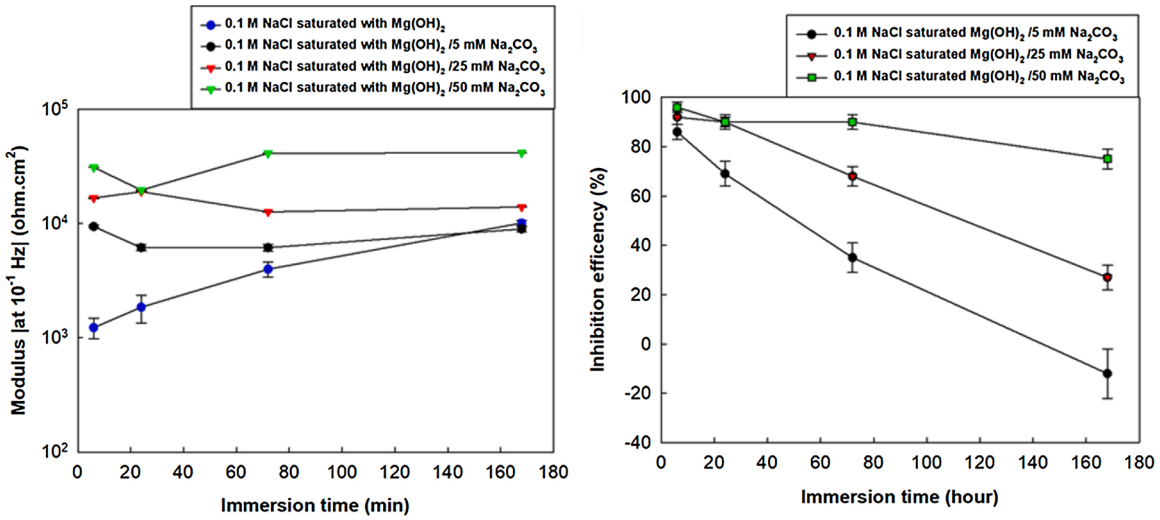

Fig. 10. Evolution of EIS fitted parameters: (a) impedance modulus at low frequency (10^{-1}Hz) (b) inhibiting efficiency.

(R_t and R_f) and a constant phase element (CPE_f and CPE_{dl}) (Fig. 8(b)). In this circuit, CPE_f and R_f are the constant phase element and resistance related to the capacitance and barrier properties of the film formed on the surface, while CPE_{dl} and R_t are correlated with the double layer capacitance and charge transfer resistance at the interface. Fig. 9 presents the fitting results of the experimental data of Fig. 7 by using the equivalent circuit of Fig. 8. The fitting results are given in Table 2.

An increase in the charge transfer resistance R_t can be observed over the time for thee substrate immersed in 0.1 M NaCl due to the growth of magnesium corrosion product. The parameters R ad L show a tendency to increase during immersion time. An inductive loop must be considered whatever the immersion time. For 5 mM Na_2CO_3 solution, the two models need to be used to fit the results with immersion time. For 6 h and 1 day of immersion, the model b (Fig. 8b) is required. The presence of a film resistance R_f is observable and increases during the first day of immersion. In addition, R_t decreases over time. After 3 days, the use of model a (Fig. 8a) is required due to the appearance of the inductive loop. For this low inhibitive concentration, the high reactivity of magnesium induced complexes phenomena which are difficult to determine by fitting analysis. For 25 mM and 50 mM Na_2CO_3 solutions, mainly an increase of the resistance charge transfer can be highlighted with immersion time and the time constant related to the formation of a protective film cannot be neglected.

For the purpose of better illustrating the inhibitive effect provided by Na_2CO_3, the impedance modulus Z (at 10^{-1} Hz) and the resulting calculated inhibiting efficiency were plotted, for all concentrations, as a function of time (up to 7 days).

In the presence of inhibitor, the reached modulus was more stable over time (Fig. 10a). After 7 days of immersion, the samples immersed in 5 mM Na_2CO_3 obtained the same |Z| value (10^4 ohm. cm^2) achieved in the absence of inhibitive species. For solutions containing 25 mM and 50 mM Na_2CO_3, the impedance modulus was much higher than in the solution containing only chlorides. The values of calculated inhibition efficiency (Eq. (5)) are given in (Fig. 10b). The inhibition efficiency curve of 5 mM Na_2CO_3 decreased significantly over time, attaining value quite close to 0 % after 7 days of immersion. For the 25 mM concentration, the decrease of the inhibition efficiency was less significant, from 95 % to 35 % after 7days. For 50 mM Na_2CO_3, the highest

Table 3
Relative composition of the extreme surface of a sample immersed for 7 days in 0.1 M NaCl saturated with $Mg(OH)_2$ without and with inhibitor determined by XPS analysis.

Element (Atomic %)	C 1 s	O 1 s	Al 2p	Mg 2p	CO_3^{2-}
0.1 M NaCl	8.37	63.51	/	28.12	3.76
0.1 M NaCl/5 mM Na_2CO_3	23.55	58.27	/	18.18	15.54
0.1 M NaCl/25 mM Na_2CO_3	25.65	58.34	/	15.36	17.19
0.1 M NaCl/50 mM Na_2CO_3	27.67	52.26	1.14	18.93	10.01

efficiencies were observed whatever the immersion time, with values reaching 97 % and 75 % after 1 h and 7 days of immersion, respectively. The decrease of the inhibition efficiency observed over time for all sodium carbonate concentrations is not related to similar decreases of |Z|, but it is rather associated to the progressive increase of the modulus in the reference solution.

3.6. Surface analysis

Surface analysis limited to the outermost surface was needed to clarify the hypothesis of the existence of a protective film comprising carbonate-based phases. The relative composition of the top-surface of AZ31 samples immersed in 0.1 M NaCl solution without or with Na_2CO_3 was determined by XPS and is displayed in Table 3.

Sodium was not detected at the extreme surfaces of both immersed samples and thus probably played no role in the protection/inhibition mechanism. On the other hand, there was a strong increase of carbon on the surface of the sample in the presence of carbonate. A small amount of aluminum was detected for the sample immersed in 50 mM of sodium carbonate. The corresponding SEM micrographs (Fig. 2(m, n, o, p)) clearly showed that the substrate was more protected in this case, making the intermetallic compounds more visible and easily detectable.

The chemical state of the elements was investigated and Fig. 11 shows the results for the sample immersed in 0.1 M NaCl saturated in $Mg(OH)_2$.

The C 1s peaks detected for binding energies of 284–289 eV (Fig. 11 (a)) are often attributed to the surface contamination [43] during air exposure. While the highest binding energy close to 290 eV is related to carbonate species [44]. Nevertheless, Table 2 shows a relative carbon composition of only 8.37 % at. of carbon. Such a low C quantity confirmed the hypothesis of surface pollution in this case.

The Mg 2p XPS spectrum for the substrate exposed to 0.1 M NaCl is shown in Fig. 11(b) and the existing peak can be associated to $Mg(OH)_2$ [45]. In order to validate these species, the Mg KLL Auger spectrum was determined Fig. 11(c). The peak detected at 305.9 eV corresponds to different corrosion products of Mg oxidized, namely, MgO, $MgCO_3$ and $Mg(OH)_2$ [46].

For all solutions with inhibitor, examination of the magnesium 2p spectra Fig. 12(b, d, f) shows that the magnesium is present as a mixture of $MgO/Mg(OH)_2$ (peak at 50.3 eV) and of $MgCO_3/Mg(OH)_2$ (peak at 51.2 eV). The C 1s peaks (Fig. 9a, c, e) detected for binding energies of 285 eV and 286.2 eV are attributed to C-C and C-O, respectively. The highest binding energy is close to 290 eV and is related to carbonate species [44]. In addition, Table 3 shows a carbon composition in the order of 25 % at. A considerable increase in the amount of carbon could therefore be observed on the AZ31 surface after immersion in the presence of the carbonate inhibitor.

3.7. Thermodynamic calculations

In order to determine if the insoluble $MgCO_3$ was thermodynamically stable under the investigated conditions, a diagram presenting the activity of species Vs pH was constructed using the Medusa Software [47]

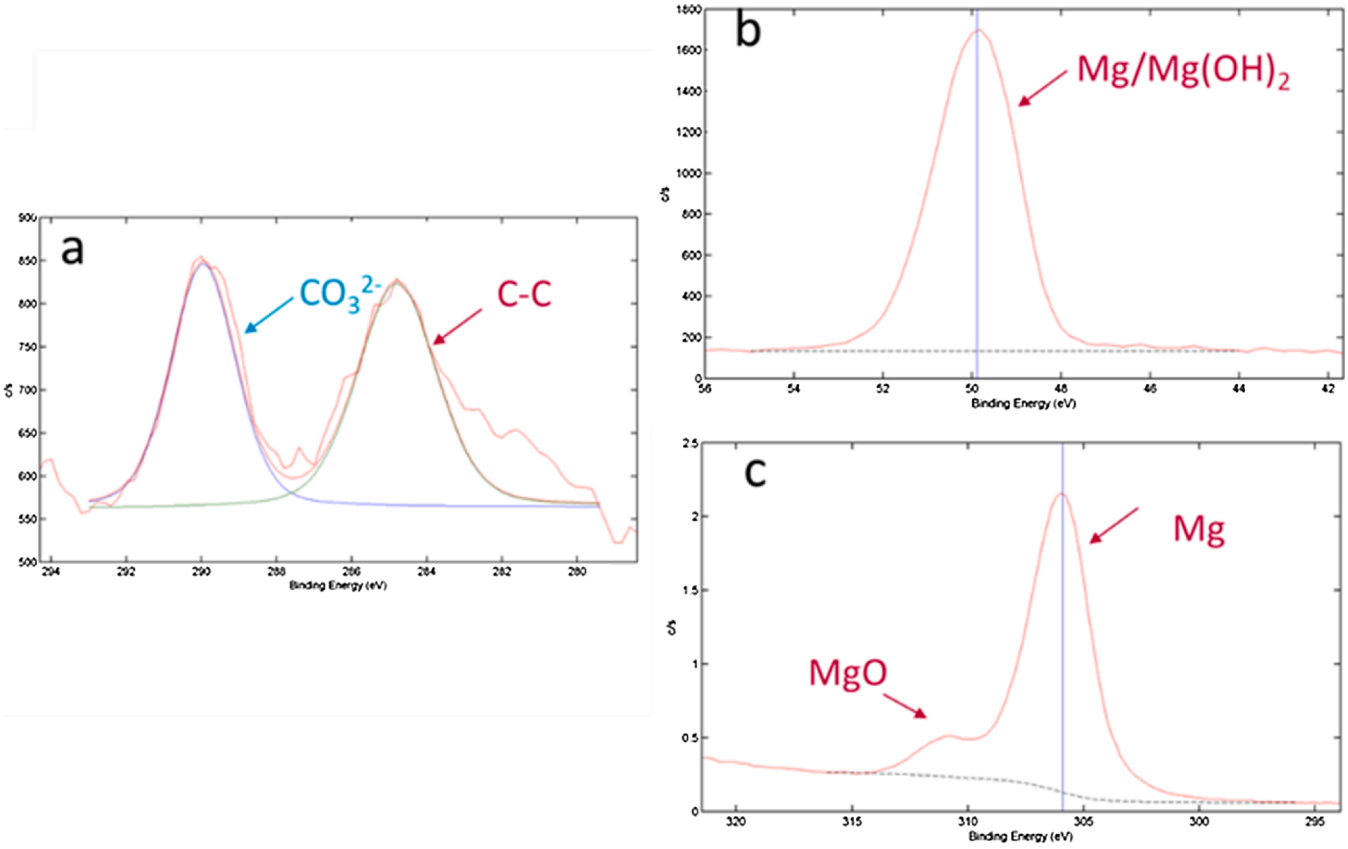

Fig. 11. Chemical state obtained by XPS analysis of the elements of AZ31 immersed for 7 days in 0.1 M NaCl saturated with $Mg(OH)_2$ without inhibitor: (a) C 1s spectrum; (b) Mg 2p spectrum; (c) Mg KLL Auger spectrum.

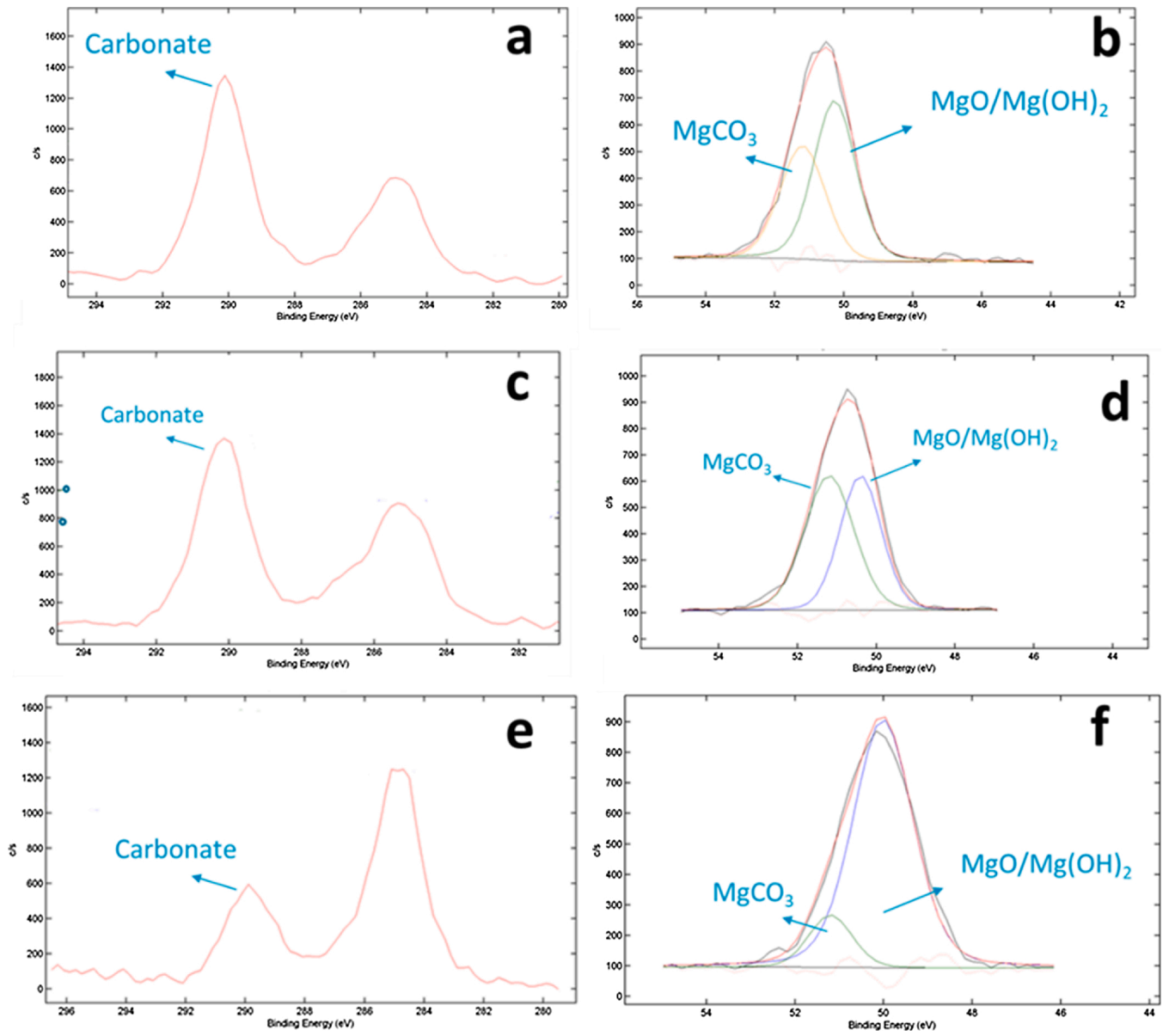

Fig. 12. Chemical states obtained by XPS analysis of the element of AZ31 immersed for 7 days in 0.1 M NaCl saturated in $Mg(OH)_2$ with 5 mM Na_2CO_3: (a) C1 s spectrum (b) Mg 2p spectrum; with 25 mM Na_2CO_3: (c) C1 s spectrum (d) Mg 2p spectrum; with 50 mM Na_2CO_3: (e) C1 s spectrum (f) Mg 2p spectrum.

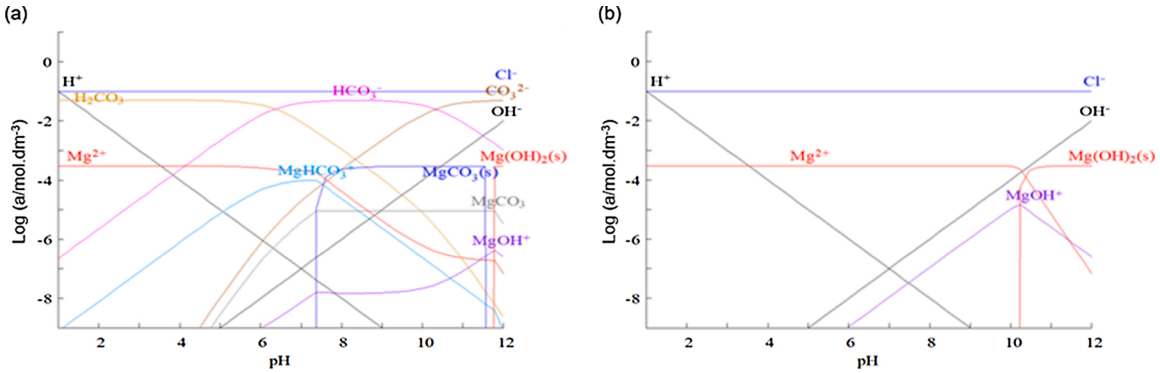

Fig. 13. (a) Logarithm of activity of the species (Vs pH) related to the corrosion of AZ31 exposed to: (a) 0.1 M NaCl +50 mM Na_2CO_3 and (b) 0.1 M NaCl (Hydra-Medusa).

(Fig. 13). The concentrations chosen for CO_3^{2-} and Cl- ions were respectively equal to 50 mM and 0.1 M, such the working solution which presented the most promising results. Lamaka et al. were able to monitor the local spatial distribution of Mg^{2+} during corrosion of AZ31 in NaCl media and concentrations between 0.3 and 0.8 mM were found. It is important to note that a solution with such high Mg^{2+} concentrations would readily precipitate $Mg(OH)_2$, since they are superior to the solubility limit of magnesium hydroxide (calculated as 0.1 mM in water at 25 °C). Therefore, the 0.3 mM Mg^{2+} (minimal value determined in their study [9]) considered in the present simulation is representative of the solution employed in this work (0.1 M NaCl saturated in $Mg(OH)_2$).

Thereby, it was possible to verify that, indeed, $MgCO_3$ was the insoluble phase presenting the highest activity from pH ~7.4 up to approximately 11.6 (Fig. 10(a)). Besides, the formation of $MgCO_{3(s)}$ was expected to increase the minimum pH required for precipitation of $Mg(OH)_2$ from ~11.3 (Fig. 13(b)) to ~11.8 (Fig. 13(a)), respectively for the non-containing and containing carbonate solutions. The relative positions of the stability ranges for both hydroxide precipitates are in accordance with simulations performed by Salgueiro et al. [48]. Furthermore, according to these authors, an eventual pH increase could be further buffered upon formation of protective $Mg(OH)_2$ phases from $MgCO_3$ (Eq. (8)):

$$MgCO_3 + H_2O + OH^- \rightarrow Mg(OH)_2 + HCO_3\text{-} \quad (8)$$

Therefore, the overall precipitation process occurring on the AZ31 surface in the presence of Na_2CO_3 is proposed according to the following reactions (Eqs. (9)–(11)). Moreover, Eq. (12) cannot be excluded, considering that XPS results showed the presence of mixture of $MgCO_3$/$Mg(OH)_2$ (Fig. 9).

$$Mg^{2+} + 2OH^- \rightarrow Mg(OH)_2 \quad (9)$$

$$MgO + H_2O \rightarrow Mg^{2+} + OH^- \rightarrow Mg(OH)_2 \quad (10)$$

$$Mg^{2+} + CO_3^{2-} \rightarrow MgCO_3 \quad (11)$$

$$2\ Mg^{2+} + CO_3^{2-} + 2OH\text{-} \rightarrow Mg_2(OH)_2CO_3 \quad (12)$$

4. Conclusion

The efficiency of sodium carbonate for the corrosion protection of AZ31 magnesium alloy was demonstrated by electrochemical measurements and supported by surface analysis and thermodynamic simulations.

Different Na_2CO_3 concentrations were tested (5 mM, 25 mM and 50 mM) in 0.1 M NaCl solution saturated in $Mg(OH)_2$ and the highest and durable inhibition efficiency was highlighted for the highest investigated carbonate concentration.

In addition, XPS analysis showed that an efficient and durable protective film comprising magnesium carbonate/hydroxycarbonate was formed on the sample surface for all concentrations of Na_2CO_3.

In summary, this study has shown that 50 mM of Na_2CO_3 protects AZ31 from corrosion in NaCl media being effective up to 7 days of immersion.

Data availability

Data will be made available on request.

CRediT authorship contribution statement

L. Prince: Conceptualization, Methodology, Validation, Formal analysis, Investigation, Writing - original draft, Visualization. **M-A. Rousseau:** Methodology, Validation, Investigation. **X. Noirfalise:** Methodology, Validation. **L. Dangreau:** Methodology, Validation. **L.B. Coelho:** Writing - review & editing, Methodology, Validation. **M.-G. Olivier:** Writing - review & editing, Supervision, Funding acquisition.

Declaration of Competing Interest

The authors report no declarations of interest.

Acknowledgment

The authors wish to thank the “Région Wallonne” in the framework of the FEDER 2014-2020 program: HYBRITIMESURF.

Appendix A. Supplementary data

Supplementary material related to this article can be found, in the online version, at doi:https://doi.org/10.1016/j.corsci.2020.109131.

References

[1] K.U. Kainer, Magnesium-alloys and Technology, Wiley, 2003.
[2] M. Esmaily, J.E. Svensson, S. Fajardo, N. Birbilis, G.S. Frankel, S. Virtanen, R. Arrabal, S. Thomas, L.G. Johansson, Fundamentals and advances in magnesium alloy corrosion, Prog. Mater. Sci. 89 (2017) 92–193, https://doi.org/10.1016/j.pmatsci.2017.04.011.
[3] J.F. King, Magnesium: commodity or exotic? Mater. Sci. Technol. 23 (2007) 1–14, https://doi.org/10.1179/174328407X154374.
[4] G. Song, A. Atrens, Understanding magnesium corrosion—a framework for improved alloy performance, Adv. Eng. Mater. 5 (2003) 837–858, https://doi.org/10.1002/adem.200310405.
[5] A. Pardo, M.C. Merino, A.E. Coy, R. Arrabal, F. Viejo, E. Matykina, Corrosion behaviour of magnesium/aluminium alloys in 3.5 wt. % NaCl, Corros. Sci. 50 (2008) 823–834, https://doi.org/10.1016/j.corsci.2007.11.005.
[6] R.M. Asmussen, W.J. Binns, R. Partovi-Nia, P. Jakupi, D.W. Shoesmith, The stability of aluminum-manganese intermetallic phases under the microgalvanic coupling conditions anticipated in magnesium alloys, Mater. Corros. 67 (2016) 39–50, https://doi.org/10.1002/maco.201508349.
[7] E. Ghali, W. Dietzel, K.U. Kainer, General and localized corrosion of magnesium alloys: A critical review, J. Mater. Eng. Perform. 22 (2013) 2875–2891, https://doi.org/10.1007/s11665-013-0730-9.
[8] N. Takeno, Atlas of Eh-pH diagrams Intercomparison of thermodynamic databases, Natl. Inst. Adv. Ind. Sci. Technol. Tokyo 285 (2005). http://scholar.google.com/scholar?hl=en&btnG=Search&q=intitle:Atlas+of+Eh-pH+diagrams+Intercomparison+of+thermodynamic+databases#0.
[9] S.V. Lamaka, O.V. Karavai, A.C. Bastos, M.L. Zheludkevich, M.G.S. Ferreira, Monitoring local spatial distribution of Mg2+, pH and ionic currents, Electrochem. Commun. 10 (2008) 259–262, https://doi.org/10.1016/j.elecom.2007.12.003.
[10] F. Cao, G.L. Song, A. Atrens, Corrosion and passivation of magnesium alloys, Corros. Sci. 111 (2016) 835–845, https://doi.org/10.1016/j.corsci.2016.05.041.
[11] S.V. Lamaka, B. Vaghefinazari, D. Mei, R.P. Petrauskas, D. Höche, M. L. Zheludkevich, Comprehensive screening of Mg corrosion inhibitors, Corros. Sci. 128 (2017) 224–240, https://doi.org/10.1016/j.corsci.2017.07.011.
[12] J. Hu, D. Huang, G. Zhang, G.-L. Song, X. Guo, Research on the inhibition mechanism of tetraphenylporphyrin on AZ91D magnesium alloy, Corros. Sci. 63 (2012) 367–378, https://doi.org/10.1016/j.corsci.2012.06.021.
[13] J.E. Gray, B. Luan, Protective coatings on magnesium and its alloys — a critical review, J. Alloys. Compd. 336 (2002) 88–113, https://doi.org/10.1016/S0925-8388(01)01899-0.
[14] S. Pommiers, J.Ô. Frayret, A. Castetbon, M. Potin-Gautier, Alternative conversion coatings to chromate for the protection of magnesium alloys, Corros. Sci. 84 (2014) 135–146, https://doi.org/10.1016/j.corsci.2014.03.021.
[15] S.Y. Wang, Q. Li, X.K. Zhong, L.Q. Li, F.N. Chen, F. Luo, Y. Dai, H. Gao, F. Liu, H. X. Zhang, Effects of NO^-_3 in NaCl solution on corrosion protection of AZ91D magnesium alloy coated with silane films, Trans. IMF 90 (2012) 78–85, https://doi.org/10.1179/174591911X13167804920948.
[16] A. Atrens, S. Johnston, Z. Shi, M.S. Dargusch, Viewpoint - understanding Mg corrosion in the body for biodegradable medical implants, Scr. Mater. 154 (2018) 92–100, https://doi.org/10.1016/j.scriptamat.2018.05.021.
[17] H. Gao, Q. Li, F.N. Chen, Y. Dai, F. Luo, L.Q. Li, Study of the corrosion inhibition effect of sodium silicate on AZ91D magnesium alloy, Corros. Sci. 53 (2011) 1401–1407, https://doi.org/10.1016/j.corsci.2011.01.008.
[18] I.A. Kartsonakis, S.G. Stanciu, A.A. Matei, E.K. Karaxi, R. Hristu, A. Karantonis, C. A. Charitidis, Evaluation of the protective ability of typical corrosion inhibitors for magnesium alloys towards the Mg ZK30 variant, Corros. Sci. 100 (2015) 194–208, https://doi.org/10.1016/j.corsci.2015.07.028.
[19] C. Lin, C. Changguo, W. Ningning, W. Jimin, D. Ling, Study of cerium and lanthanum conversion coatings on AZ63 magnesium alloy surface, Rare Met. Mater. Eng. 44 (2015) 333–338, https://doi.org/10.1016/S1875-5372(15)30030-8.

[20] G. Williams, H.N. McMurray, R. Grace, Inhibition of magnesium localised corrosion in chloride containing electrolyte, Electrochim. Acta 55 (2010) 7824–7833, https://doi.org/10.1016/j.electacta.2010.03.023.
[21] F.E.-T. Heakal, O.S. Shehata, N.S. Tantawy, Enhanced corrosion resistance of magnesium alloy AM60 by cerium(III) in chloride solution, Corros. Sci. 56 (2012) 86–95, https://doi.org/10.1016/j.corsci.2011.11.019.
[22] R. Lindström, L.G. Johansson, G.E. Thompson, P. Skeldon, J.E. Svensson, Corrosion of magnesium in humid air, Corros. Sci. 46 (2004) 1141–1158, https://doi.org/10.1016/j.corsci.2003.09.010.
[23] S. Feliu, C. Maffiotte, A. Samaniego, J.C. Galván, V. Barranco, Effect of the chemistry and structure of the native oxide surface film on the corrosion properties of commercial AZ31 and AZ61 alloys, Appl. Surf. Sci. 257 (2011) 8558–8568, https://doi.org/10.1016/j.apsusc.2011.05.014.
[24] D. Nam, D. Lim, S.-D. Kim, D. Seo, S.E. Shim, S.-H. Baeck, The fabrication of a conversion film on AZ31 containing carbonate product and evaluation of its corrosion resistance, J. Alloys. Compd. 737 (2018) 597–602, https://doi.org/10.1016/j.jallcom.2017.12.061.
[25] M. Esmaily, M. Shahabi-Navid, J.-E. Svensson, M. Halvarsson, L. Nyborg, Y. Cao, L.-G. Johansson, Influence of temperature on the atmospheric corrosion of the Mg–Al alloy AM50, Corros. Sci. 90 (2015) 420–433, https://doi.org/10.1016/j.corsci.2014.10.040.
[26] H. Liu, F. Cao, G.-L. Song, D. Zheng, Z. Shi, M.S. Dargusch, A. Atrens, Review of the atmospheric corrosion of magnesium alloys, J. Mater. Sci. Technol. (2019), https://doi.org/10.1016/j.jmst.2019.05.001.
[27] Q. Qu, J. Ma, L. Wang, L. Li, W. Bai, Z. Ding, Corrosion behaviour of AZ31B magnesium alloy in NaCl solutions saturated with CO2, Corros. Sci. 53 (2011) 1186–1193, https://doi.org/10.1016/j.corsci.2010.12.014.
[28] A. Atrens, G.L. Song, F. Cao, Z. Shi, P.K. Bowen, Advances in Mg corrosion and research suggestions, J. Magnes. Alloy 1 (2013) 177–200, https://doi.org/10.1016/j.jma.2013.09.003.
[29] E. Gulbrandsen, Anodic behaviour of Mg in HCO−3/CO2−3 buffer solutions. Quasi-steady measurements, Electrochim. Acta 37 (1992) 1403–1412, https://doi.org/10.1016/0013-4686(92)87014-Q.
[30] Y. Xin, K. Huo, H. Tao, G. Tang, P.K. Chu, Influence of aggressive ions on the degradation behavior of biomedical magnesium alloy in physiological environment, Acta Biomater. 4 (2008) 2008–2015, https://doi.org/10.1016/j.actbio.2008.05.014.
[31] R.-C. Zeng, Y. Hu, S.-K. Guan, H.-Z. Cui, E.-H. Han, Corrosion of magnesium alloy AZ31: The influence of bicarbonate, sulphate, hydrogen phosphate and dihydrogen phosphate ions in saline solution, Corros. Sci. 86 (2014) 171–182, https://doi.org/10.1016/j.corsci.2014.05.006.
[32] J. Yang, C. Blawert, S.V. Lamaka, K.A. Yasakau, L. Wang, D. Laipple, M. Schieda, S. Di, M.L. Zheludkevich, Corrosion inhibition of pure Mg containing a high level of iron impurity in pH neutral NaCl solution, Corros. Sci. 142 (2018) 222–237, https://doi.org/10.1016/j.corsci.2018.07.027.
[33] G. Song, A. Atrens, M. Dargusch, Influence of microstructure on the corrosion of diecast AZ91D, Corros. Sci. 41 (1998) 249–273, https://doi.org/10.1016/S0010-938X(98)00121-8.
[34] Z. Shi, A. Atrens, An innovative specimen configuration for the study of Mg corrosion, Corros. Sci. 53 (2011) 226–246, https://doi.org/10.1016/j.corsci.2010.09.016.
[35] S. Feliu, I. Llorente, Corrosion product layers on magnesium alloys AZ31 and AZ61: surface chemistry and protective ability, Appl. Surf. Sci. 347 (2015) 736–746, https://doi.org/10.1016/j.apsusc.2015.04.189.
[36] G. Baril, C. Blanc, N. Pébère, AC impedance spectroscopy in characterizing time-dependent corrosion of AZ91 and AM50 magnesium alloys characterization with respect to their microstructures, J. Electrochem. Soc. 148 (2001) B489, https://doi.org/10.1149/1.1415722.
[37] Y. Zhang, C. Yan, F. Wang, W. Li, Electrochemical behavior of anodized Mg alloy AZ91D in chloride containing aqueous solution, Corros. Sci. 47 (2005) 2816–2831, https://doi.org/10.1016/j.corsci.2005.01.010.
[38] F. Cao, Z. Shi, J. Hofstetter, P.J. Uggowitzer, G. Song, M. Liu, A. Atrens, Corrosion of ultra-high-purity Mg in 3.5 % NaCl solution saturated with Mg(OH)2, Corros. Sci. 75 (2013) 78–99, https://doi.org/10.1016/j.corsci.2013.05.018.
[39] M. Curioni, L. Salamone, F. Scenini, M. Santamaria, M. Di Natale, A mathematical description accounting for the superfluous hydrogen evolution and the inductive behaviour observed during electrochemical measurements on magnesium, Electrochim. Acta 274 (2018) 343–352, https://doi.org/10.1016/j.electacta.2018.04.116.
[40] G. Song, D.S.T. John, J. Nairn, The anodic dissolution of magnesium and sulphate solutions in chloride, Corros. Sci. 39 (1997) 1981–2004, https://doi.org/10.1016/S0010-938X(97)00090-5.
[41] A. Samaniego, B.L. Hurley, G.S. Frankel, On the evidence for univalent Mg, J. Electroanal. Chem. 737 (2015) 123–128, https://doi.org/10.1016/j.jelechem.2014.04.013.
[42] S. Lebouil, O. Gharbi, P. Volovitch, K. Ogle, Mg dissolution in phosphate and chloride electrolytes: insight into the mechanism of the negative difference effect, Corrosion 71 (2015) 234–241, https://doi.org/10.5006/1459.
[43] L. Wang, T. Shinohara, B.-P. Zhang, XPS study of the surface chemistry on AZ31 and AZ91 magnesium alloys in dilute NaCl solution, Appl. Surf. Sci. 256 (2010) 5807–5812, https://doi.org/10.1016/j.apsusc.2010.02.058.
[44] H. Yao, Y. Li, A.T. Wee, An XPS investigation of the oxidation/corrosion of melt-spun Mg, Appl. Surf. Sci. 158 (2000) 112–119, https://doi.org/10.1016/S0169-4332(99)00593-0.
[45] M. Santamaria, F. Di Quarto, S. Zanna, P. Marcus, Initial surface film on magnesium metal: a characterization by X-ray photoelectron spectroscopy (XPS) and photocurrent spectroscopy (PCS), Electrochim. Acta 53 (2007) 1314–1324, https://doi.org/10.1016/j.electacta.2007.03.019.
[46] Y. BOUVIER, Use of an Auger parameter for characterizing the Mg chemical state in different materials, Surf. Coatings Technol. 180–181 (2004) 169–173, https://doi.org/10.1016/j.surfcoat.2003.10.062.
[47] I. Puigdomenech, Hydra/Medusa chemical equilibrium database and plotting software, KTH R. Inst. Technol. (2004). Google scholar.
[48] M. Salgueiro Azevedo, C. Allély, K. Ogle, P. Volovitch, Corrosion mechanisms of Zn (Mg,Al) coated steel: The effect of HCO3− and NH4+ ions on the intrinsic reactivity of the coating, Electrochim. Acta 153 (2015) 159–169, https://doi.org/10.1016/j.electacta.2014.09.140.